

Light 'Higgs', yet strong interactions

This content has been downloaded from IOPscience. Please scroll down to see the full text.

2014 J. Phys. G: Nucl. Part. Phys. 41 025002

(<http://iopscience.iop.org/0954-3899/41/2/025002>)

View [the table of contents for this issue](#), or go to the [journal homepage](#) for more

Download details:

IP Address: 147.96.14.16

This content was downloaded on 06/03/2014 at 13:42

Please note that [terms and conditions apply](#).

Light ‘Higgs’, yet strong interactions

**Rafael L Delgado, Antonio Dobado
and Felipe J Llanes-Estrada**

Departamento de Física Teórica I, Universidad Complutense de Madrid,
E-28040 Madrid, Spain

E-mail: dobado@fis.ucm.es

Received 17 September 2013

Published 20 January 2014

Abstract

The claimed finding of a light Higgs boson makes the minimal Standard Model unitary. Yet, we recall that the general low-energy dynamics for the minimal electroweak symmetry breaking sector with three Goldstone bosons and one light scalar is not so. We construct the effective Lagrangian for these four particles and their scattering amplitudes, that can be extracted from LHC experiments when longitudinal W , Z modes be properly isolated for $E \gg M_W$ (equivalence theorem). We then observe the known increase in interaction strength with energy and explore various unitarization methods in the literature in the absence of other new physics (as LHC experiments fail to report anything up to 600 GeV). Our generic conclusion is that for most of parameter space the high-energy scattering of the longitudinal W 's is strongly interacting (with the Minimal Standard Model a remarkable exception). We find and study a second σ -like scalar pole of the $W_L W_L$ amplitude.

Keywords: unitarity, Higgs boson, strong interactions

(Some figures may appear in colour only in the online journal)

1. Introduction

Both CMS [1] and ATLAS [2] have reported an excess of events in a four-lepton (largely 4μ) spectra compatible with a minimal Standard Model (MSM) Higgs boson, with a claimed statistical significance of signal over a background around 5σ . The two collaborations have also reported possible excesses in the two-photon [3] and WW [4, 5] channels, though these are less clear to us due to the uncalculated backgrounds. There are various other hints and claims by the same and other collaborations that are at too early a stage to draw definite conclusions.

Most importantly, the examination of numerous channels has revealed no evidence of additional new physics up to 600 GeV, although searches continue [6].

If the situation settles in the existence of only one Higgs-like boson at low energies, then the electroweak symmetry breaking sector (EWSBS) of the Standard Model (SM) is composed

of this scalar resonance and the three would-be Goldstone bosons (WBGB). With help of the global symmetry breaking pattern $SU(2)_L \times SU(2)_R \rightarrow SU(2)_C$, it is easy to write down the effective electroweak chiral Lagrangian (EWChL) [7] for the three WBGB's in a similar way as it is done in standard chiral perturbation theory (ChPT) for pions [8]. At energies sufficiently higher than 100 GeV (their typical mass scale), we can identify them with the longitudinal components of the W and Z bosons, thanks to the equivalence theorem [9], which allows us to experimentally access them. The separation of the transverse and longitudinal modes of the W 's now seems very promising with the LHC data [10].

We then couple the recently discovered new scalar φ to the WBGB in a standard way and thus write down the most general effective Lagrangian describing the low-energy dynamics of these four modes [11, 38, 42, 43] in section 2. It is interesting to realize that the fact that we have discovered four scalar light modes with a strong gap (no further states until at least about 600 GeV) strongly suggests that we should seriously take the possibility that these scalars are to be interpreted as the Goldstone bosons (GB) corresponding to some spontaneous symmetry breaking happening in the EWSBS at some higher scale f [12].

In the main part of this article, we first concentrate on the 'high' energy behavior of the scattering amplitudes for the longitudinal components of the electroweak gauge bosons (EWGB) or equivalently WBGB's. Here, we mean $M_W, M_\varphi = O(100 \text{ GeV}) \ll E$, but we will consider at most $E \simeq \Lambda \simeq 4\pi v \simeq 3 \text{ TeV}$ since the validity of effective approaches is not granted at still higher energies.

The perturbative amplitudes are given in section 3, as are also the partial wave expansions and the coupled-channel formalism connecting the $W_L W_L$ and $\varphi\varphi$ channels. The low-energy Lagrangian contains two parameters, $v = 246 \text{ GeV}$ (that breaks the electroweak symmetry) and f which typically represents a higher scale still undetermined. In the MSM, $f = v$ and only one parameter is necessary to describe the interaction. In this case, the Higgs saturates unitarity; but if $f \neq v$, the elastic scattering WBGB amplitude, proportional to $s = E_{\text{cm}}^2$, eventually grows out of the unitarity bound. Then, the perturbative description loses its validity as the interactions become strong. In addition, there is a prominent inelastic reaction $W_L W_L \rightarrow \varphi\varphi$ controlled by two additional parameters (pure numbers, denoted α and β below) and the pure scalar potential with parameters λ_3, λ_4 . If $\alpha^2 = \beta$, the channels decouple, otherwise their coupling also grows with the square of the energy.

We then use different techniques to unitarize the effective low-energy amplitudes in a physically sensible way to higher energies in section 4. We do not commit to a specific microscopic model [13] of the high-energy theory such as Composite Higgs, Walking Technicolor (see for example the second article in [11] and references therein), an electroweak scale Dilaton [14] or others, but instead employ generally valid approaches such as dispersion relations [15, 16] and on-shell factorization [17] (algebraic unitarization formulae).

Our conclusion is that, save for the exception of the MSM, the scattering amplitudes become characteristically strong at the TeV scale and unitarization is needed. When projecting over s -wave and analytically continuing to the second Riemann sheet, we find a broad pole, very reminiscent of the renowned scalar σ , that provides for central attraction of the nuclear potential in QCD, with several numerical computations shown in section 5. We discuss whether one can or not think of it as an additional particle, and if so why is it interesting, in section 6, where we also wrap our discussion.

2. Generic effective Lagrangian

In the spirit of the previous discussion, we adopt the most general Lagrangian describing the low-energy dynamics of the four light modes (three w WBGB and the Higgs φ). This can

be written as a $SU(2)_L \times SU(2)_R/SU(2)_C = SU(2) \simeq S^3$ nonlinear sigma model (NLSM) coupled to a scalar field φ in leading order of the derivative chiral expansion, as

$$\mathcal{L} = \frac{v^2}{4} g(\varphi/f) \text{Tr}(D_\mu U)^\dagger D^\mu U + \frac{1}{2} \partial_\mu \varphi \partial^\mu \varphi - V(\varphi), \quad (1)$$

where U is a field taking values in the $SU(2)$ coset and that we will parameterize as $U = \sqrt{1 - \tilde{\omega}^2/v^2} + i\tilde{\omega}/v$, with $\tilde{\omega} = \omega_a \tau^a$ the WBGB; $D_\mu U = \partial_\mu U + W_\mu U - U Y_\mu$, $W_\mu = -g i W_\mu^i \tau^i/2$, $Y_\mu = -g' i B_\mu^i \tau^3/2$ coupling the transverse gauge bosons; $v = 246$ GeV the MSM Higgs-doublet vacuum expectation value (or in terms of Fermi's weak constant, $v^2 = 1/(\sqrt{2}G_F)$); f is an arbitrary, new, dynamical energy scale needed for the generic dynamics of the EWSBS; $g(x)$ is an arbitrary analytical functional of the scalar field

$$g(\varphi/f) = 1 + \sum_{n=1}^{\infty} g_n \left(\frac{\varphi}{f} \right)^n = 1 + 2\alpha \frac{\varphi}{f} + \beta \left(\frac{\varphi}{f} \right)^2 + \dots, \quad (2)$$

where only the first terms are relevant for this work and we have parameterized them in terms of two arbitrary α and β real constants instead of the more common a and b in [11]. This is because we are using the scale f instead of v to normalize the scalar field φ , which we consider more appropriate for our work here. Obviously, we have $a = \alpha v/f$ and $b = \beta v^2/f^2$.

If we accept at face value the WW data from CMS and ATLAS [4, 5] (while also keeping in mind various experimental caveats¹), the parameter f/α (equivalently, a) is constrained to 95% confidence level (2σ) to lie within the respective experimental bands

$$\frac{f}{\alpha} \in (225, 350) \text{ GeV} \text{ or } a \in (0.70, 1.1) \text{ (CMS)} \quad (3)$$

$$\frac{f}{\alpha} \in (185, 285) \text{ GeV} \text{ or } a \in (0.87, 1.3) \text{ (ATLAS)}. \quad (4)$$

These can be extracted from figures 7(b) and 13 of [5] and [4], respectively, that bind the ratio between the hWW coupling quotiented by its value in the SM, or κ_v , so that $f/\alpha = v/\kappa_v$, assuming other parameters are kept fixed at their SM value. Nevertheless, in our numeric computations below, we will explore a broader range of values of f/α in case these bounds are relaxed by later, more accurate data and because of the intrinsic theoretical interest of the calculation. No relevant (order $O(1)$) constraint on β is known to us, because no two-Higgs final state has yet been detected.

In addition, some authors have combined the results of the two experiments (in spite of the different systematics) or made theory-assisted analysis that can be found in [19]. The possible bounds on the a and b parameters, or alternatively f and b , are then somewhat different. It is also worth mentioning that an analysis of the LEP precision observables [18] (though dependent on a loop-cutoff parameter that entails a large degree of arbitrariness) is consistent with equation (3) and (4), yielding (assuming a positive a -parameter)

$$\frac{f}{\alpha} \in (205, 270) \text{ GeV} \text{ or } a \in (0.91, 1.2) \text{ LEP} \quad (5)$$

at 99% confidence level.

¹ Very strong background subtractions are needed, and the background functions are not known from first principles. Instead the backgrounds are fitted in off mass-peak control regions and then extrapolated to the signal zone of 125 GeV employing Monte Carlo simulations. The 'transfer factors' for these extrapolations depend on parton distribution functions, QCD corrections, and Monte Carlo model choices. ATLAS posits an error varying from only 2% for no-jet WW events to $O(50\%)$ for events with two or more jets. In addition, the zero-width approximation is adopted for the Higgs and the Standard Model tensor structure is assumed in the analysis.

Finally, V is an arbitrary analytical potential for the scalar field,

$$V(\varphi) = \sum_{n=0}^{\infty} V_n \varphi^n \equiv V_0 + \frac{M_\varphi^2}{2} \varphi^2 + \sum_{n=3}^{\infty} \lambda_n \varphi^n \quad (6)$$

in obvious notation.

The Lagrangian written in this simple, canonical form of equation (1), encodes the low-energy dynamics of any model fulfilling the simple hypothesis of having only four light modes coming from the EWSBS, in terms of a few parameters.

The most obvious and paradigmatic example is simply the MSM [20] which can be obtained by just setting $f = v$, $\alpha = \beta = 1$, $g_i = 0$ for $i \geq 3$ and by identifying the Higgs field H with φ so that $M_H^2 = M_\varphi^2 = 2\lambda v^2$, and the scalar self-couplings as $\lambda_3 = \lambda v$, $\lambda_4 = \lambda/4$ and $\lambda_i = 0$ for $i \geq 4$. The function g is given by

$$g_{\text{MSM}}(\varphi/v) = \left(1 + \frac{\varphi}{v}\right)^2. \quad (7)$$

A second, very interesting, family of models includes those in which the scalar resonance is understood as the GB associated with the spontaneous breaking of the approximate scale (and conformal) invariance of the unknown symmetry breaking sector, i.e., those that identify the light scalar as a dilaton [14]. The g function is similar to that of the MSM but with the new scale f playing the role of v

$$g_{\text{dilaton}}(\varphi/f) = \left(1 + \frac{\varphi}{f}\right)^2 \quad (8)$$

and in its simplest version, the potential is given by:

$$V(\varphi) = \frac{M_\varphi^2}{4f^2} (\varphi + f)^2 \left[\log \left(1 + \frac{\varphi}{f}\right) - \frac{1}{4} \right] \quad (9)$$

but more complicated potentials are also possible, depending on the precise form of the breaking of conformal invariance. Obviously in these dilaton models, one has $\alpha = \beta = 1$ and in general $f \neq v$.

A third type of model that can be treated with equation (1) is that in which the WBGB and the scalar are considered as the GB associated with some spontaneous global symmetry breaking. For example, one possibility is to consider the coset $SO(5)/SO(4) = S^4$ [21] coming from a symmetry breaking from $SO(5)$ to $SO(4)$ at some scale f , which provides exactly four GB, followed by a second breaking from $SO(4)$ to $SO(3)$ at the electroweak scale v . This is typical of Composite Higgs models in 4D or with extra dimensions, and in this case

$$g_{\text{CHM}}(\varphi/f) = \frac{f^2}{v^2} \sin^2 \left(\theta + \frac{\varphi}{f} \right), \quad (10)$$

where $\sin \theta = v/f$, and various Composite Higgs models can be selected by appropriately choosing the potential $V(\varphi)$.

The Lagrangian density in equation (1) provides the scattering amplitudes among the four light particles. The high-energy ($s \gg M_\varphi^2$) scattering of the WBGB is related to the scattering of the longitudinal components of the electroweak bosons through the equivalence theorem,

$$T(\omega^a \omega^b \rightarrow \omega^c \omega^d) = T(W_L^a W_L^b \rightarrow W_L^c W_L^d) + O\left(\frac{M_W}{\sqrt{s}}\right), \quad (11)$$

and thus $|T|^2$ is observable. Therefore, we will concentrate on the WBGB scattering for $M_\varphi^2, M_W^2, M_Z^2 \ll s < \Lambda^2$, where Λ is some ultraviolet (UV) cutoff of about 3 TeV, setting the limits of applicability of the effective theory. In order to expose the increased strength of the

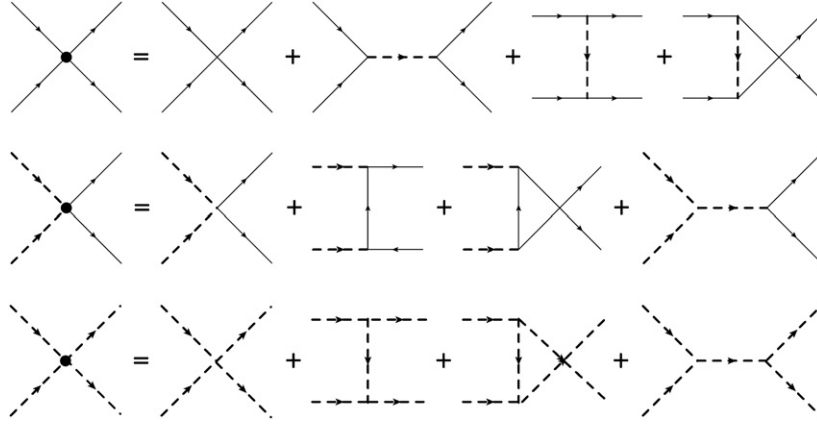


Figure 1. Feynman diagrams for the tree-level scattering amplitudes of WBGB's (related to W_L by the equivalence theorem) and a light scalar φ .

interaction, it suffices to treat the scalar dynamics alone, so we will turn off the transverse electroweak gauge fields by setting $g = g' = 0$. Then, equation (1) can be written as

$$\mathcal{L} = \frac{1}{2}g(\varphi/f)\partial_\mu\omega^a\partial^\mu\omega^b\left(\delta_{ab} + \frac{\omega^a\omega^b}{v^2 - \omega^2}\right) + \frac{1}{2}\partial_\mu\varphi\partial^\mu\varphi - \frac{1}{2}M_\varphi^2\varphi^2 - \lambda_3\varphi^3 - \lambda_4\varphi^4 + \dots \quad (12)$$

Notice that by rescaling f and redefining β in a trivial way, it is possible to set $\alpha = 1$ in equation (2) without losing generality,

$$g(\varphi/f) = 1 + 2\frac{\varphi}{f'} + \beta'\left(\frac{\varphi}{f'}\right)^2 + \dots \quad (13)$$

in which case the bands on f/α equations (3) and (4) give directly the interval of f' values (around v) that are temptatively viable in view of experimental data. This leaves two free parameters affecting the WBGB's in our energy region of interest (the redefined f and β), and two more (λ_3, λ_4) in the scalar self-potential V , assuming that the scalar mass M_φ is now as hinted from experiment; we set $M_\varphi \simeq 125$ GeV. However, in the following, we will still keep the explicit α -dependence in our formulae so that we can easily trace it for comparison with previous works. In particular, the old EWChL without any Higgs-like light resonance corresponds to $\alpha = \beta = 0$. Nevertheless, our numerical results presented in section 5 are all obtained with $\alpha = 1$. Also, as customary in this context, it will be useful to introduce the adimensional parameter $\xi = v^2/f^2$ so that $\xi = 1$ corresponds to the MSM.

3. Scattering in perturbation theory

3.1. Feynman amplitudes

With the Lagrangian density in equation (12), it is now straightforward to obtain the tree-level scattering amplitudes among the four particles that appear at low-energies. The corresponding Feynman diagrams are represented in figure 1.

First of all, we have the WBGB elastic scattering amplitude, usually parameterized in terms of one function $A(s, t, u)$, which in this particular case is a function of s only:

$$T_{abcd}^{2\omega 2\omega} = A(s)\delta_{ab}\delta_{cd} + A(t)\delta_{ac}\delta_{bd} + A(u)\delta_{ad}\delta_{bc}, \quad (14)$$

where

$$A(s) = \frac{s}{v^2} \left(1 + \xi \alpha^2 \frac{s}{M_\phi^2 - s} \right), \quad (15)$$

which for the MSM case $\xi = \alpha = 1$ leads to the well known result

$$A(s) = \frac{s}{v^2} \frac{1}{1 - s/M_H^2}. \quad (16)$$

In the massless scalar limit, we obtain the low-energy theorem (LET),

$$A_0(s) = (1 - \xi \alpha^2) \frac{s}{v^2}, \quad (17)$$

which is a generalization, including the new light scalar boson, of the one given in [22]. Interestingly enough, this amplitude vanishes only in the particular case of the MSM. This fact is an indication of the weakly interacting nature of the Higgs sector for $M_H \simeq 125$ GeV. However, in the general case with two scales v, f and $\xi \neq 1$, the amplitude increases linearly with s , suggesting the possibility of having a strongly interacting scenario. This observation triggers the rest of our investigation.

Next, we consider the inelastic process $\omega^a \omega^b \rightarrow \varphi \varphi$ or its inverse $\varphi \varphi \rightarrow \omega^a \omega^b$ which have the same amplitude because of the assumed time-reversal invariance of the EWSBS sector.

The tree-level inelastic amplitude is

$$T_{ab}^{2\omega 2\varphi} = -\frac{\delta_{ab}}{f^2} \left[\beta s + \alpha^2 \frac{(M_\phi^2 - t)^2}{t} + \alpha^2 \frac{(M_\phi^2 - u)^2}{u} + \frac{6\alpha\lambda_3 f s}{s - M_\phi^2} \right]. \quad (18)$$

In the massless scalar limit, one gets

$$T_{ab}^{2\omega 2\varphi} = -\frac{\delta_{ab}}{f^2} [\beta s + \alpha^2(t + u) + 6\alpha\lambda_3 f]. \quad (19)$$

By using the on-shell relation $s + t + u = 0$, we see that this amplitude is proportional to λ_3 in the particular case $\alpha^2 = \beta$, which includes the MSM and dilaton models. However, typically the constants λ_i are of the order of M_ϕ^2 and then we have $T_{ab}^{2\omega 2\varphi} = 0$ in the massless scalar limit. Thus, for dilaton-type models, it is a very good approximation in practice to neglect the channel coupling and concentrate only on the elastic $\omega\omega$ amplitude. Nevertheless, we shall handle the coupling to keep the discussion generic.

The third independent amplitude, scalar-scalar scattering $\varphi\varphi \rightarrow \varphi\varphi$, is again elastic and given by

$$T^{2\varphi 2\varphi} = -24\lambda_4 - 36\lambda_3^2 \left(\frac{1}{s - M_\phi^2} + \frac{1}{t - M_\phi^2} + \frac{1}{u - M_\phi^2} \right) \quad (20)$$

and again we see that $T^{2\varphi 2\varphi} = 0$ in the massless scalar limit. Therefore, in this limit, only the elastic WBGB survives, with amplitude linear in s provided that ξ is different from one, i.e., the MSM excepted. This is clearly an indication for strongly interacting WBGB scattering as a generic property of any model different from the MSM.

For full generality, one should notice that the WBGB interaction is not exactly linear as in equation (17). Following the philosophy of the EWChL, it is also possible to add to the original Lagrangian density (1) higher derivative terms. For example, one could add the four derivative terms

$$\mathcal{L}_4 = a_4 (Tr V_\mu V_\nu)^2 + a_5 (Tr V_\mu V^\mu)^2, \quad (21)$$

where $V_\mu = D_\mu U U^\dagger$. These terms produce additional contributions to the tree-level EWGB scattering of order s^2 , and bring-in dependence on two new adimensional parameters a_4 and a_5 which of course depend on the underlying dynamics producing the spontaneous electroweak symmetry breaking. Following the philosophy of the EWChL, these new terms should be added to the previous leading term at high energies proportional to s in the WBGB scattering amplitude. However, a complete consistent treatment requires also the computation of loops which are also of the order of s^2 as it was done a long time ago in [23]. The EWChL parameters a_4 and a_5 require renormalization which in turn makes them dependent on an arbitrary renormalization scale μ in such a way that this dependence compensates the one coming from the one-loop $\log(-s/\mu^2)$ to make the total WBGB amplitude μ independent.

3.2. Partial waves

The tree-level amplitudes are not appropriate descriptions much above thresholds since they do not respect unitarity. In the following, we will introduce and compare different methods for improving the unitary behavior of the amplitudes. Since the unitarity relation is simplest for each partial-wave amplitude, it is convenient to introduce the angular expansion

$$t_{IJ}(s) = \frac{1}{64\pi} \int_{-1}^1 d(\cos \theta) P_J(\cos \theta) T_I(s, \cos \theta), \quad (22)$$

where $P_J(\cos \theta)$ are the Legendre polynomials, θ is the scattering angle in the center of mass frame and T_I are the (custodial) isospin amplitudes. From now on, we will concentrate in the (iso) scalar channel $I = J = 0$. Then, for the WBGB scattering, we have:

$$T_0^{2\omega 2\omega} = 3A(s) + A(t) + A(u) \quad (23)$$

and $P_0 = 1$. For the process $\omega^a \omega^b \rightarrow \varphi \varphi$, $T_0^{2\omega 2\varphi} = \sum_a T_{aa}^{2\omega 2\varphi} / \sqrt{3}$ and for $\varphi \varphi \rightarrow \varphi \varphi$, obviously $T_0^{2\varphi 2\varphi} = T^{2\varphi 2\varphi}$. It is simple enough to find the corresponding (iso) scalar amplitudes as

$$t_{2\omega 2\omega}(s) = \frac{s}{32\pi v^2} \left(2 + \frac{3\xi \alpha^2 s}{M_\varphi^2 - s} \right) + \frac{\xi \alpha^2}{32\pi v^2} \left[s - 2M_\varphi^2 + \frac{2M_\varphi^4}{s} \log \left(1 + \frac{s}{M_\varphi^2} \right) \right],$$

$$t_{2\omega 2\varphi}(s) = t_{2\varphi 2\omega}(s) = -\frac{\sqrt{3}s}{32\pi f^2} \left(\beta - \frac{6\alpha \lambda_3 f}{M_\varphi^2 - s} \right) + \frac{\sqrt{3}\alpha^2}{3} 2\pi f^2 \left[s + 2M_\varphi^2 - \frac{2M_\varphi^4}{s\sigma} \log \left(\frac{2M_\varphi^2 - s(1 - \sigma)}{2M_\varphi^2 - s(1 + \sigma)} \right) \right],$$

and

$$t_{2\varphi 2\varphi}(s) = -\frac{1}{16\pi} \left(12\lambda_4 - \frac{18\lambda_3^2}{M_\varphi^2 - s} \right) - \frac{9\lambda_3^2}{4\pi s\sigma^2} \log \left(\frac{2M_\varphi^2 - s(1 - \sigma^2)}{2M_\varphi^2 - s(1 + \sigma^2)} \right), \quad (24)$$

where $\sigma = \sqrt{1 - 4M_\varphi^2/s}$.

3.3. Coupling channels

The perturbative amplitudes found in the previous subsection have the well known left cuts (LC) coming from the angular integration of the crossed channels which start in different points for each channel due to the different thresholds. However, as they are tree-level real partial waves in the physical region, they do not carry the full analytical structure; they lack an imaginary part for physical s , and they do not have a right cut (RC) starting at threshold.

Notice that unitarity here is a non-trivial requirement, coupling the three amplitudes in a nonlinear way.

To simplify the discussion, and also because we are mainly interested in the region $M_\varphi^2 \ll s$, we will work with a slightly simplified version of the partial waves, corresponding to the asymptotic behavior in the $M_\varphi^2/s \ll 1$ regime. This approximation will not only simplify the equations a bit, but more importantly it will make all of the LC thresholds coincide at $s = 0$, which will be important in the following to avoid mixing of the LC and RC cuts in the coupled-channel unitarized amplitudes. Then, we will be using the approximate tree-level partial waves:

$$t_\omega(s) = \frac{1}{16\pi v^2} \left[s(1 - \xi\alpha^2) - \xi\alpha^2 M_\varphi^2 + \xi\alpha^2 \frac{M_\varphi^4}{s} \log\left(\frac{s}{M_\varphi^2}\right) \right], \quad (25)$$

$$t_{\omega\varphi}(s) = t_{\varphi\omega}(s) = \frac{\sqrt{3}(\alpha^2 - \beta)s}{32\pi f^2} + \frac{\sqrt{3}\alpha^2}{16\pi f^2} \left[M_\varphi^2 + \frac{2M_\varphi^4}{s} \log\left(\frac{s}{M_\varphi^2}\right) \right] \quad (26)$$

and

$$t_\varphi(s) = \frac{9\lambda_3^2}{4\pi s} \log\left(\frac{s}{M_\varphi^2}\right) - \frac{3\lambda_4}{4\pi}, \quad (27)$$

where we have used the simplified notation $\omega = 2\omega 2\omega$, $\omega\varphi = 2\omega 2\varphi$ and $2\varphi 2\varphi = \varphi$.

The above amplitudes are grouped into the tree-level reaction matrix

$$T = \begin{pmatrix} t_\omega & t_{\omega\varphi} \\ t_{\varphi\omega} & t_\varphi \end{pmatrix}. \quad (28)$$

3.4. The electroweak chiral Lagrangian approach

The tree-level amplitudes can be approached in a different way by considering the limit $M_\varphi^2 \simeq M_W^2 \simeq M_Z^2 \ll s$ which is appropriate for applying the effective theory ideas. Instead of starting from a nonlinear σ -like model, one can adopt the power-counting of the EWChL, that we now quickly apply to the case of one additional Higgs-like scalar φ : In this case, the low-energy partial waves become

$$\begin{aligned} t_0^\omega &= \frac{s}{16\pi v^2} (1 - \xi\alpha^2) \\ t_0^{\omega\varphi} &= \frac{\sqrt{3}(\alpha^2 - \beta)s}{32\pi f^2} \\ t_0^\varphi &= 0 \end{aligned} \quad (29)$$

which are the order s LETs. However, following the philosophy of the EWChL, one should also add order s^2 contributions to the WBGB partial wave. To this order, we have tree-level contributions coming from the four derivative terms of the effective Lagrangian discussed at the end of subsection III.A proportional to a_4 and a_5 . Also, we have to add the one-loop corrections with WBGB and φ internal lines which are also of order s^2 . Of course the one-loop integral is divergent but the divergences can be regulated, for example by using dimensional regularization, and reabsorbed by the a_i couplings which become renormalized couplings $a_i(\mu)$ depending on an arbitrary renormalization scale μ . Then, the total NLO contribution can be written as:

$$t_1^\omega = s^2 \left[A(\mu) + D \log\left(\frac{s}{\mu^2}\right) + E \log\left(\frac{-s}{\mu^2}\right) \right], \quad (30)$$

where

$$A(\mu) = A_0 + \frac{7a_4(\mu) + 11a_5(\mu)}{12\pi v^4}. \quad (31)$$

Here, A_0 is a constant depending on the particular regularization scheme used (we will show the details of the computation elsewhere [24]). D and E are two constants tuned with $A(\mu)$ so that the amplitude is μ independent i.e.:

$$A(\mu) = A(\mu_0) + (D + E) \log \frac{\mu^2}{\mu_0^2}. \quad (32)$$

This partial wave is formally similar to the one found in [23] but the constants are different because now the light scalar resonance φ contributes to the sum over intermediate states at one loop. These constants can be obtained from the results found in the very complete recent work [25] where the one-loop scattering amplitudes, including the Higgs-like scalar and WBGB, are computed. Using perturbative unitarity, we have

$$\text{Im } t_1^\omega = |t_0^\omega|^2 + |t_0^{\omega\varphi}|^2 = \left(\frac{s}{16\pi v^2}\right)^2 \left[(1 - \xi\alpha^2)^2 + \frac{3}{4}(\alpha^2 - \beta)^2 \xi^2 \right]. \quad (33)$$

On the other hand, from equation (30) above:

$$\text{Im } t_1^\omega = -E\pi s^2 \quad (34)$$

so that

$$E = -\frac{\pi}{(4\pi v)^4} \left[(1 - \xi\alpha^2)^2 + \frac{3}{4}(\alpha^2 - \beta)^2 \xi^2 \right]. \quad (35)$$

Thus, the EWChL prediction for the amplitude is:

$$t_\chi^\omega = t_0^\omega + t_1^\omega + \mathcal{O}(s^3/v^3). \quad (36)$$

This partial wave has better unitary and analytical properties than the tree-level amplitude t_0^ω having the proper LC. However, unitarity is only realized perturbatively or in other words:

$$\text{Im } t_\chi^\omega = |t_\chi^\omega|^2 + \mathcal{O}(s^3/v^3). \quad (37)$$

We see below how this result from EWChL approach can be enormously improved by the use of the so called inverse amplitude method (IAM).

Another important comment is that in the particular but paradigmatic case of the MSM, $v = f$ (or $\xi = 1$), and the whole EWChL approach does not make sense reflecting that the MSM with a light Higgs is unitary but weakly interacting at the energy we are interested in here, i. e. $s \gg M_\varphi^2$.

4. Unitarized scattering amplitudes

The unitarity condition for the exact reaction matrix \tilde{T} for massless particles reads

$$\text{Im } \tilde{T} = \tilde{T} \tilde{T}^\dagger \quad (38)$$

on the physical region, i.e., just above the RC where $s = |s| + i\epsilon$. There are in the literature different ways for incorporating exact unitarity to a given approximate amplitude and a lot of controversy about which method is more appropriate or even the level of arbitrariness of all of them. To extract model-independent features, we will therefore make use of several of the known methods, that we treat in the following subsections.

4.1. *K*-matrix, algebraic unitarization and strength of channel-coupling interaction

Starting from a tree amplitude, probably the simplest unitarization is the so called *K*-matrix method [26]. In our simple case, this amounts to defining the unitarized reaction matrix as $\tilde{T} = T(1 - iT)^{-1}$ which obviously satisfies the unitarity condition for real, positive s , since $T = T^T = T^\dagger$. However, this new matrix does not have the proper analytical structure since in particular it lacks a RC. This is a displeasing drawback since physical amplitudes cannot have poles in the first, or physical, Riemann sheet. The RC opens the door to analytical prolongation to the second Riemann sheet where poles belong and may be found and understood as dynamically generated resonances, so important in strongly interacting scenarios. For this reason, we will rather define our unitarized matrix, (often called *K* matrix in the literature), as

$$\tilde{T} = T(1 - JT)^{-1}, \quad (39)$$

where $J(s)$ is the function

$$J(s) = -\frac{1}{\pi} \log \left(\frac{-s}{\Lambda^2} \right), \quad (40)$$

and Λ some UV cutoff. This function provides the proper analytical structure to \tilde{T} with the RC needed for analytical prolongation to the second Riemann sheet. In addition, $\text{Im} J = 1$ on the RC so that the unitarity condition is exactly fulfilled. Possible resonances can show up as roots of the determinant $\Delta = \det(1 - JT)$, or in other words, they solve

$$\Delta = 1 - J(t_\omega + t_\varphi) + J^2(t_\omega t_\varphi - t_{\omega\varphi}^2) = 0 \quad (41)$$

on the second Riemann sheet².

Since the key concern is the WBGB scattering amplitude, we write down the unitarity condition for a particular partial wave

$$\text{Im} \tilde{t}_\omega = \tilde{t}_\omega \tilde{t}_\omega^* + \tilde{t}_{\omega\varphi} \tilde{t}_{\omega\varphi}^*. \quad (42)$$

This equation is exactly fulfilled by the corresponding given angular-momentum matrix element of reaction matrix \tilde{T} of equation (39),

$$\tilde{t}_\omega = \frac{t_\omega - J(t_\omega t_\varphi - t_{\omega\varphi}^2)}{1 - J(t_\omega + t_\varphi) + J^2(t_\omega t_\varphi - t_{\omega\varphi}^2)}. \quad (43)$$

In figure 4, in section 5 below, we show that the effect of the coupled $\varphi\varphi$ channel on the $W_L W_L$ channel is small, in the particular case $\beta = 1$, as can also be seen analytically. As we have already pointed out, the partial waves $t_{\omega\varphi}$ and t_φ are then suppressed when $M_\varphi^2 \ll s$, the energy region of interest in this work. This means that $t_{\omega\varphi}$ and t_φ are subleading with respect to t_ω and therefore one could expect to have:

$$\text{Im} \tilde{t}_\omega \simeq \tilde{t}_\omega \tilde{t}_\omega^* \quad (44)$$

on the RC and this is indeed the case, as also checked numerically in figure 4.

From equation (29), it is clear that for $\beta = \alpha^2$, the WBGB are very weakly coupled to the scalars $\varphi\varphi$ and one can consider the WBGB elastic scattering alone. However, in the more general situation $\beta \neq \alpha^2$, the WBGB can be strongly coupled to the $\varphi\varphi$ state and then a coupled-channel formalism is needed to study the $\omega\omega$ interactions. For the particular but

² The amplitude in equation (39) can be thought of as the resummation of the relativistic Lippmann–Schwinger series with the scattering calculated at one loop. Normally, this would lead to integral expressions, but the purely algebraic expression in which T and J are factorized (no potentials inside the loop integrals) is a feature of effective theories with polynomial expansions, called on-shell factorization (the off-shell, non-factorizable parts are proportional to tree-level diagrams and can be reabsorbed in the corresponding parameters) [17].

interesting case $\beta = \alpha^2$ (elastic case), the K-matrix unitarized partial wave t_ω reduces to the simple algebraic formula

$$\tilde{t}_\omega = \frac{t_\omega}{1 - Jt_\omega}. \quad (45)$$

Now we can again take $M_\phi \simeq 125$ GeV, leaving only as free parameter the new scale f . Notice that this case includes in particular all dilaton models.

We have now sufficient theory to address the interesting question of when the interactions are either weak or strong, and the question of whether any poles appear in the second Riemann sheet of the amplitude.

Advancing generic results of section 5, we can see for example in figures 6 and 7 that for any value of f not too close to v , we are typically in a strongly interacting regime (with partial wave with modulus of order one) and also produce a pole in the second Riemann sheet. In QCD, setting $\xi = 0$ and $v = f_\pi$ in the LET for $A_0(s)$ above, we would be reproducing a K-matrix unitarized first order ChPT for pions in the chiral limit and then the found resonance would be just the σ -meson [27].

However, as we can see in figure 9, the width corresponding to the pole found is in general too large to be considered a real resonance, but still produces such huge enhancement of the scattering, that it leads to a strong-interaction regime for most conceivable f -values. The exception is the region $f \simeq v$. This precisely corresponds to the renormalizable MSM. Of course the MSM with a light Higgs of 125 GeV is obviously weakly interacting.

The surprise is that in the larger class of models considered in this work, that one needs to examine following the effective-theory philosophy, this weakly interacting behavior is quite rare since a kind of fine-tuning $f = v$ is needed to avoid the generic strongly interacting scenario.

4.2. Alternative unitarization: large N limit

Equation (39), the core of the K-matrix method, is in the end a model. Although it incorporates the correct low-energy amplitude and is by construction unitary and has the correct RC, it entails an on-shell factorization (JT is an algebraic matrix product and not an integral operator product) that is strictly true only for polynomial interactions, and the LC is only treated perturbatively. These are very sensible approximations that capture the main physics for physical s and have been very successful in many cases. Still, it is very important to explore other ways to unitarize the high-energy WBGB scattering amplitude, to discard artifacts of the unitarization method and give more robustness to our general results.

In this subsection, we rederive an interesting alternative for the computation of the amplitudes, treating them in the large- N limit (where N refers to the number of GBs). This is a non perturbative approximation which was introduced for the linear sigma model (LSM) [29] but it can also be extended to the NLSM [30]. Being non perturbative, the large- N approximation produces, even at lowest order, amplitudes which have good unitarity and analytical behavior so that they do not need any further unitarization. The main idea is to extend the original minimal coset for a weak isospin triplet plus a scalar singlet, $SO(4)/SO(3) = S^3$, to $SO(N+1)/SO(N) = S^N$ so that we now have N WBGB and one scalar. Now one can consider the limit $N \rightarrow \infty$ simultaneously with $v \rightarrow 0$ keeping v^2/N fixed (and at the end evaluate the leading formulae thus obtained at $N = 3$).

One proceeds by expanding the amplitudes in powers of $1/N$, and in the simplest approach one can keep just the first non-trivial term. Starting from the tree-level amplitude for WBGB

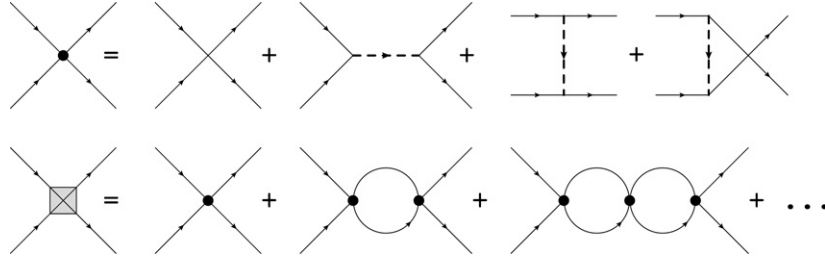


Figure 2. Feynman diagrams for large N scattering WBGB's (related to W_L by the equivalence theorem) and a light scalar φ .

elastic scattering $A(s)$, and taking into account that v^2 is of order N , the amplitude A_N , correct to order $1/N$, is given by a Lippmann–Schwinger series

$$A_N = A - A \frac{NI}{2} A + A \frac{NI}{2} A \frac{NI}{2} A - A \frac{NI}{2} A \frac{NI}{2} A \frac{NI}{2} A + \dots, \quad (46)$$

where $I = I(s)$ is the simple two body loop integral:

$$I(s) = \int \frac{d^4 q}{(2\pi)^4} \frac{i}{q^2(q+p)^2} = \frac{1}{16\pi^2} \log\left(\frac{-s}{\Lambda^2}\right) = -\frac{1}{8\pi} J(s) \quad (47)$$

and where p is the total momentum so that $p^2 = s$; we have introduced the UV cutoff Λ ; N counts the number of WBGB in the loop; and the factors $1/2$ are combinatorial factors because of the indistinguishability of the WBGB. It is immediate to check that all the terms in the series are of order $1/N$. Now it is possible to formally sum the geometric series yielding

$$A_N(s) = \frac{A(s)}{1 + \frac{NI(s)A(s)}{2}}. \quad (48)$$

The corresponding Feynman diagrams are represented in figure 2.

The isospin scalar amplitude is given in this case by:

$$T_0^\omega = NA(s) + A(t) + A(u) \quad (49)$$

so in the large N limit only the s channel contributes. Thus, the (iso)scalar partial wave for elastic WBGB scattering, t_N^w , is just

$$t_N^\omega(s) = \frac{t_0^\omega}{1 - J t_0^\omega}, \quad (50)$$

where

$$t_0^\omega(s) = \frac{sN}{32\pi v^2} \left(1 + \xi \alpha^2 \frac{s}{M_\varphi^2 - s} \right). \quad (51)$$

It is amazing to realize how similar this partial wave and the one obtained from the K-matrix method are. Even if they are not identical for $N = 3$, as seen comparing equation (45) with equation (51), the geometric-series structure of equations (45) and (50), coming from the right s -channel cut dominating over the t -channel cut for physical s (much closer to the RC), is the same. Thus, they give rise to qualitatively and quantitatively similar results for $s \gg M_\varphi^2$ as can be seen in figure 11.

We thus find that the large- N approximation provides strong support to the scenario of strongly interacting scattering for the WBGB that we obtain, under the general condition $f \neq v$, from the simple K-matrix amplitude in subsection 4.1.

Finally it is interesting to notice that in the large- N limit, the decoupling of the $\omega\omega$ and $\varphi\varphi$ channels occurs in a natural way, because the φ loops are suppressed by a factor N with respect to the WBGB loops. So here, the values of β and λ_i in the $V(\varphi)$ potential are irrelevant to the strength of the $t^{\omega\varphi}$ interaction, that is weak due to the large- N approximation.

4.3. Alternative unitarization: the N/D method: algebraic treatment

To further check that indeed our results are generic, and not contingent on the algebraic K-matrix formalism, we will also use the N/D method for unitarizing the elastic t^ω scalar partial wave, directly in the elastic case (i.e. we decouple the $\varphi\varphi$ channel by restricting ourselves to $\beta = \alpha^2$).

We will try to unitarize the perturbative tree-level elastic $\omega\omega$ partial wave, $t^\omega(s)$, calculated in section 3. The full \tilde{t}^ω amplitude satisfies a dispersion relation given its imaginary parts on the LC, RC as well as the contribution of any CDD poles or subtraction constants that may be necessary.

The N/D method is a (non-unique) construction that solves the dispersion relation satisfied by the partial-wave amplitude $\tilde{t}^\omega(s)$ starting with an ansatz as [28, 31]

$$\tilde{t}^\omega(s) = \frac{N(s)}{D(s)}, \quad (52)$$

where the numerator function $N(s)$ carries the amplitude's left hand cut, so that $\text{Im } N(s > 0) = 0$, and the denominator function $D(s)$ carries the right hand one, and $\text{Im } D(s < 0) = 0$. This gives the quotient $\tilde{t}^\omega(s)$ the expected analytical structure. Therefore, $\text{Im } N(s) = 0$ on the RC and $\text{Im } D(s) = 0$ on the LC. In addition, elastic unitarity requires $\text{Im } D(s) = -N(s)$ on the RC and also we have $\text{Im } N(s) = D(s) \text{Im } \tilde{t}^\omega(s)$ on the LC.

The dispersive representation of \tilde{t}^ω usually entangles the left and RCs (as known since the Kramers–Kronig equations in electrodynamics) but the N/D ansatz simplifies the system to two equations that are sequentially solved, one to be satisfied by $N(s)$, and one yielding $D(s)$ once $N(s)$ has been calculated.

In once-subtracted form, using the normalization $D(0) = 1$, we have

$$D(s) = 1 - \frac{s}{\pi} \int_0^\infty \frac{ds' N(s')}{s'(s' - s - i\epsilon)} \quad (53)$$

$$N(s) = \frac{s}{\pi} \int_{-\infty}^0 \frac{ds' \text{Im } N(s')}{s'(s' - s - i\epsilon)}, \quad (54)$$

where we have set to zero the subtraction constant in the equation for $N(s)$ ($N(0) = 0$). Once solved, the complete amplitude is constructed as $\tilde{t}^\omega(s) = N(s)/D(s)$. As usual with dispersive approaches, these two equations encode the requirement of analyticity (hence causality) but they do not determine the amplitude since they have many solutions. However, starting from some approximated $N(s)$, we can iterate these equations to find an improved amplitude with better analytical and unitary properties. For example, we can start from some approximate $N_0(s)$ and using equation (53) we obtain $D_0(s)$. Then, we can use equation (54) to get $N_1(s)$ and so on. This iteration is known to converge very quickly [32] in many cases, so we will just consider here the lowest order approximation $t^\omega(s) \simeq N_0(s)/D_0(s)$ with $N_0(s)$ being the tree-level amplitude. As the integrals diverge at large and small s and we employ an IR cutoff m^2 and an UV cutoff Λ^2 in lieu of a more sophisticated subtraction scheme.

Quite remarkably, it is possible to carry out all integrations of this first iteration analytically for the scalar channel that we are treating, as we now show, delaying some computational details to the [appendix](#).

We find

$$D_0(s) = 1 - \frac{s}{\pi} \int_{m^2}^{\Lambda^2} \frac{ds' t_\omega(s')}{s'(s' - s - i\epsilon)} = 1 - \frac{M_\varphi^2}{32\pi^2 v^2} x I(x), \quad (55)$$

where $x = s/M_\varphi^2$ and we have introduced the dispersive integral

$$I(x) = \int_{x_1}^{x_2} \frac{dx'}{x' - x - i\epsilon} \left[2 + \xi - \frac{2\xi}{x'} + \frac{3\xi x'}{1 - x'} + \frac{2\xi}{x'^2} \log(1 + x') \right] \quad (56)$$

with the dimensionless $x_1 = m^2/M_\varphi^2$ and $x_2 = \Lambda^2/M_\varphi^2$ IR and UV regulators. This integral can be split in four pieces $I = I_1 + I_2 + I_3 + I_4$ for ease of handling. The first is

$$I_1 = (2 + \xi) \log \frac{x_2 - x}{x_1 - x}. \quad (57)$$

Notice that, because of $x_1 \leq x \leq x_2$, I_1 develops an imaginary part on the RC. The same happens to the following integrals too.

$$I_2 = \frac{2\xi}{x} \log \frac{x_2(x_1 - x)}{x_1(x_2 - x)}, \quad (58)$$

$$I_3 = \frac{3\xi}{1 - x} \left(x \log \frac{x_2 - x}{x_1 - x} - \log \frac{1 - x_2}{1 - x_1} \right) \quad (59)$$

and finally

$$I_4 = \frac{2\xi}{x} \left\{ \frac{\log(1 + x_2)}{x_2} - \frac{\log(1 + x_1)}{x_1} - \log \frac{x_2}{1 + x_2} + \log \frac{x_1}{1 + x_1} \right. \\ \left. + \frac{1}{x} [Li_2(-x_2) - Li_2(-x_1)] + \frac{1}{x} \left[\log(1 + x_2) \log \frac{x - x_2}{1 + x} \right. \right. \\ \left. \left. - \log(1 + x_1) \log \frac{x - x_1}{1 + x} + Li_2 \left(\frac{1 + x_2}{1 + x} \right) - Li_2 \left(\frac{1 + x_1}{1 + x} \right) \right] \right\}, \quad (60)$$

where we have assumed $x_1 > 1$ to avoid the zeroes of the $x - 1$ denominators. From the $I_1 \dots I_4$ integrals, it is not difficult to show explicitly that over the RC,

$$\text{Im } D_0 = -N_0 = -t^\omega, \quad (61)$$

and therefore, since $\tilde{t}^\omega = D_0/N_0$, we see that one-channel unitarity over the physical RC is respected,

$$\text{Im } \tilde{t}^\omega = |\tilde{t}^\omega|^2. \quad (62)$$

Thus, \tilde{t}^ω is an unitary partial wave with the appropriate analytical structure including its LC and the most important RC. It is then possible to continue analytically to the second Riemann sheet where dynamical resonances could show up as poles at some $s_0 = M^2 - i\Gamma M$ (with mass and width interpretation reliable as long as s_0 is not very far from the real axis, so that $\Gamma \ll M$).

4.4. The inverse amplitude method

In section 3.4, we saw that the EWChL approach provides the first terms of a power series expansion for the WBGB scattering amplitude in s/v^2 . The first two terms construct a partial wave which has good analytical properties but still is unitary only in the perturbative sense. However, the truncated series can be regarded in a much more efficient way by using the so called IAM. This method was introduced in the context of ordinary ChPT for pions [33] providing a fully unitarized amplitude with the right analytical structure that can be prolonged to the second Riemann sheet and is therefore able to reproduce dynamical resonances as poles in this second sheet. The use of this method has made possible to fit an enormous set of meson scattering data, including resonances, in terms of a few chiral parameters. Because the EWChL has the same formal structure as the ordinary ChPT one, the application of this method can

be extended to this case too [34] (see also [35] for a complete review of both applications of the IAM). It is based on the dispersion relation fulfilled by the algebraic inverse of the partial waves resulting in exact treatment of the RC contribution and a perturbative estimation of the LC one. After some quite general assumptions concerning the absence of zeros in the original amplitudes³, the final result is a very practical expression:

$$\tilde{t}^\omega = \frac{t_0^\omega}{1 - \frac{t_0^\omega}{t_1^\omega}}. \quad (63)$$

As already mentioned, this amplitude is exactly unitary and it has the proper analytical structure including the LC and the RC with $\text{Im } \tilde{t}^\omega = |\tilde{t}^\omega|^2$ on it. The analytical continuation to the second sheet may or may not have poles in the different channels (putative resonances) depending on the values of the renormalized chiral parameters a_4 and a_5 , as studied in [34] for the case of no light Higgs-like resonance and more recently in [37] for the case of the MSM with a light Higgs.

From the very definition of the IAM method and the form of EWChL amplitudes, the position of the poles in the second Riemann sheet s_0 fulfill the equation

$$\frac{16\pi v^2 s_0}{1 - \xi \alpha^2} (A(s_0) + iE(\text{Arg}(s_0) - \pi)) = 1, \quad (64)$$

where we have chosen the renormalization scale μ as the pole position s_0 for the sake of simplicity, using the fact that s_0 , as any observable, is μ independent. Since $\alpha = 1$, for $\xi \rightarrow 1$ ($f \rightarrow v$), the pole that produces strong interactions is removed to infinite mass, returning the weakly-interacting MSM.

5. Numerical results

In this section, we offer several typical numerical results obtained with the different unitarization methods that we have introduced. As we will see, even if some numerical details are different, the qualitative behavior of the amplitudes and their analytical continuation to the second Riemann sheet of s are similar.

5.1. Improved K matrix approach

In figure 3, we show the unitarized $|\tilde{t}_w|$ (the WBGB scattering amplitude) that fails to satisfy unitarity unless the second channel is included (also shown in the figure for a generic $\alpha = 1$, $\beta \neq 1$ taken as $\beta = 3$, with $\xi \simeq 1/4$, $\lambda_3 = M_\varphi^2/f$, and $\lambda_4 = M_\varphi^2/f^2$). This is due to the strong interchannel coupling. In the same figure 3, we plot, in addition to $|\tilde{t}_w|^2$ (bottom line), $|\tilde{t}_w|^2 + |\tilde{t}_{\omega\varphi}|^2$ and $\text{Im}(\tilde{t}^\omega)$ (top two lines). The latter two are on top of each other, establishing coupled-channel unitarity. Notice that all the interactions are strong in this generic case.

The situation is simpler for $\beta = \alpha^2 (=1)$ because the tree-level amplitude $t_{\omega\varphi}$ fails to have a term proportional to s and then it is not strongly interacting anymore. As shown in figure 4, for $f \neq v$, the modulus of the elastic amplitude $|t_\omega|$ is large and of order 1 for TeV energies. The scalar-scalar interaction remains perturbative since it is controlled by λ_3 and λ_4 which are typically of order M_φ^2/f and M_φ^2/f^2 that, for $f > v$, is even weaker than in the standard model case. Finally, the smallest amplitude corresponds to the interchannel coupling $t_{\omega\varphi}$. Thus, for values of β near $\alpha^2 = 1$, it is a good approximation to neglect the coupled channels and use the one-channel equation (45) instead of equation (43).

³ The error incurred by ignoring the subthreshold Adler-zeroes in the simple formula in equation (63) has been corrected for by calculating without this simplification [36], and found to be below the per-mille level for physical s .

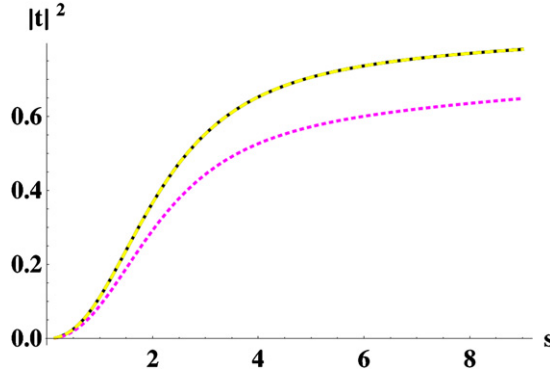


Figure 3. Square modulus of the unitarized t_ω (bottom, dashed line) that fails to satisfy single-channel unitarity for $\alpha = 1$, $\beta = 3$. On the contrary, the sum of the squared scattering s-wave amplitude over the two open channels $|t_\omega|^2 + |t_{\omega\phi}|^2$ falls on top of $\text{Im } t_\omega$ (top two lines, solid and dotted), showing how coupling channels is needed to restore unitarity. See the particular values of the different parameters considered in the main text.

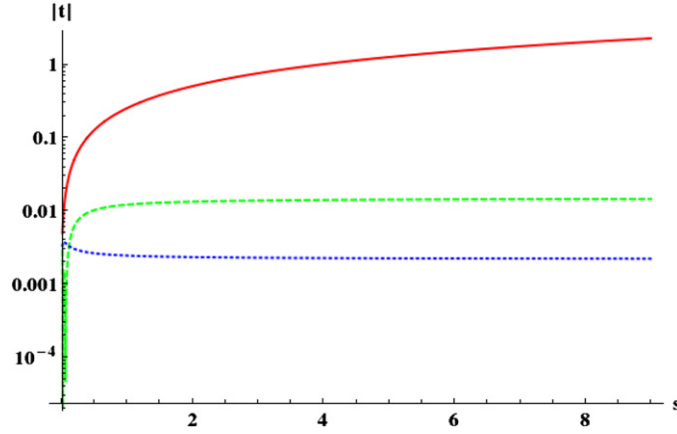


Figure 4. We show the small effect of the coupled channels with the tree-level amplitudes in equation (25) for moderate β of order $\alpha^2 = 1$. As seen, the amplitude for $\omega\omega$ scattering (solid line at the top, red online) is much larger than that for the $\phi\phi$ channel (dashed line in the middle, green online) and the interchannel coupling amplitude is smallest (dotted line at the bottom, blue online). Parameters used: $f = 2v$, $\beta = \alpha^2 = 1$, $\lambda_3 = M_\phi^2/f$, $\lambda_4 = M_\phi^2/f^2$. The OX axis represents Mandelstam s in TeV^2 .

Notice that even if we can neglect interchannel coupling, whenever $\beta = \alpha^2$ (or simply $\beta = 1$ since, as mentioned above, we can always redefine f and β so that $\alpha = 1$), we will find strong interaction and the need for unitarizing the $\omega\omega$ elastic scattering amplitude. Our results are then in broad agreement with other typical works [39, 40] that considered $W_L W_L$ elastic scattering and also found heavier resonances due to the strong interaction developing.

As seen in figure 5, unitarity is violated by t_ω whose modulus exceeds 1 slightly before $\sqrt{s} = 2$ TeV for the given parameter set. Since this scattering amplitude between WBGB is thus found to be strong, the tree-level approximation breaks down and some unitarization method is required to have a realistic amplitude usable in comparisons with future experimental data in $\omega\omega$ elastic scattering.

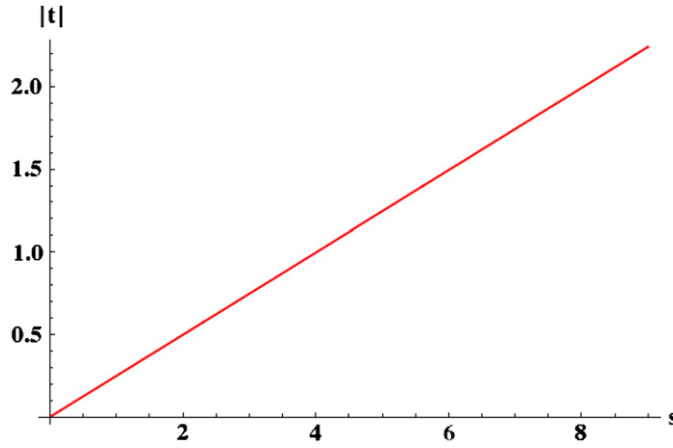


Figure 5. Modulus of the tree-level t_ω from equation (24) for physical s showing the violation of unitarity for $f \neq v$. Axes and parameters as in figure. 4.

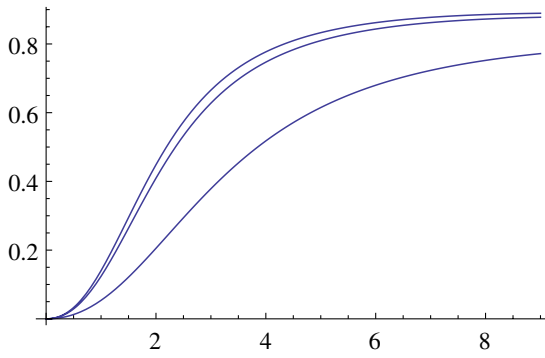


Figure 6. Modulus of the unitarized t_ω from equation (45) for physical s showing that, for $f \neq v$, the appropriately unitarized interactions are strong (with modulus of order 1). We swipe several values of f . From top to bottom, $f = 1.2$ TeV, $f = 0.8$ TeV and $f = 0.4$ TeV (with $\Lambda = 3$ TeV, $\mu = 100$ GeV regulating the loop integral).

We therefore unitarize the amplitude, as in equation (45), and plot it in figure 6, that is acceptable from the point of view of unitarity, though the interaction is strong (with $|t_\omega| = \mathcal{O}(1)$).

The amplitude modulus in figure 6 is indeed characteristic of strong interactions. We have numerically checked that the outcome of the program satisfies $\text{Im } t = |t|^2$ for null interchannel coupling, and equation (38) for finite interchannel coupling.

In figure 6, we see that the dependence in f is not very pronounced unless $f \simeq v$ (we will analyze this dependence in more detail in subsection 5.3 below).

Among the various reasons why a low-energy interaction can be strong is a pole in the scalar channel, as the $f_0(500)$ or σ now well established in $\pi\pi$ scattering. Such pole of the t_ω amplitude in the second Riemann sheet is mandated by a zero of equation (41). We have found such scalar pole, that is clearly visible in figures 7 and 8.

To complete the analysis, we have followed the motion of the pole at s_0 in the complex s plane. If the pole admits a resonance interpretation (a dubious case for such broad structures

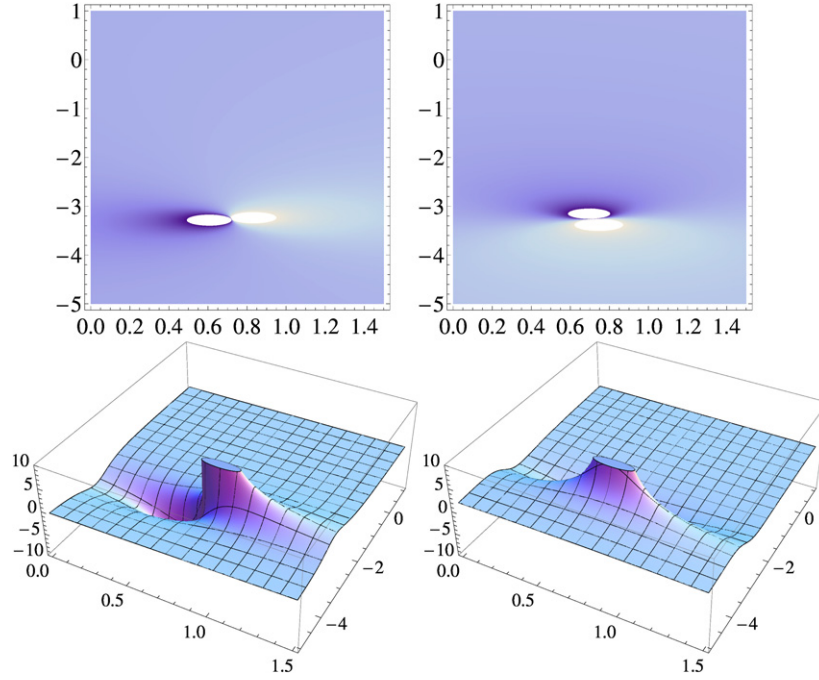


Figure 7. By extending s to the second Riemann sheet, we find that the amplitude presents a pole very far off from the physical axis, reminiscent of the σ meson of $\pi\pi$ scattering. Top: two-dimensional contour plots in the complex s -plane. Bottom: amplitude against complex- s (real part starting at 0, imaginary part on the second Riemann sheet for negative values, axis units in TeV). The left plots show the real part of the amplitude $\text{Re}t^\omega(s)$ and the right plots the imaginary part $\text{Im}t^\omega(s)$. Here, we take $f = 400$ GeV not that much larger than v .

as we find), then one can interpret $\text{Re}(s) = M^2$, $\text{Im}(s) = -M\Gamma$. We plot such ‘mass’ and ‘width’ in figure 9 for various values of f .

The pole position is seen to stabilize, for $f \gg v$, around 810 GeV. The width is so broad (above 2 TeV) that one can hardly talk of a resonance. Thus, although within reach of the LHC for large values $f \gg v = 246$ GeV, the extraction of the pole from experimental data will have to be dispersive, by first extracting the amplitude t_ω and then prolonging s to the complex plane; an attempt to obtain a Breit–Wigner resonant width from experimental data will yield very model-dependent results.

A very interesting numerical exercise is to keep λ_3, λ_4 small as above, so that the $\varphi\varphi$ interaction is perturbative; make $f = 260$ GeV $\simeq v$, so that t_ω is also perturbative for all the relevant low-energy range, but choose $\beta = 3$ so that the interchannel coupling is strong. Then, we generate a strong, resonant interaction between the $\omega\omega$ and $\varphi\varphi$ channels that dynamically generates a so called ‘coupled-channel resonance’, a pole on the second Riemann sheet of Mandelstam’s s that is absent if we take $\beta \rightarrow \alpha^2 = 1$, but is there for larger coupling. This effect is clearly visible in figure 10.

5.2. Large N

In figure 11, we compare the result of the large- N amplitude in equation (50) with the K-matrix approach in equation (45) and see how comparable the two amplitudes are, in

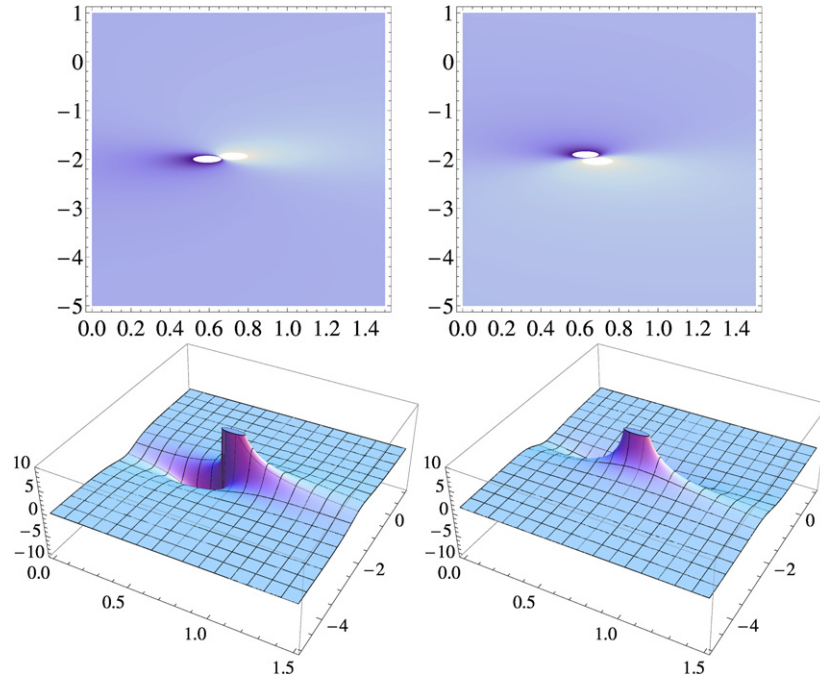


Figure 8. Same as in figure 7 but increasing the scale to $f = 4$ TeV.

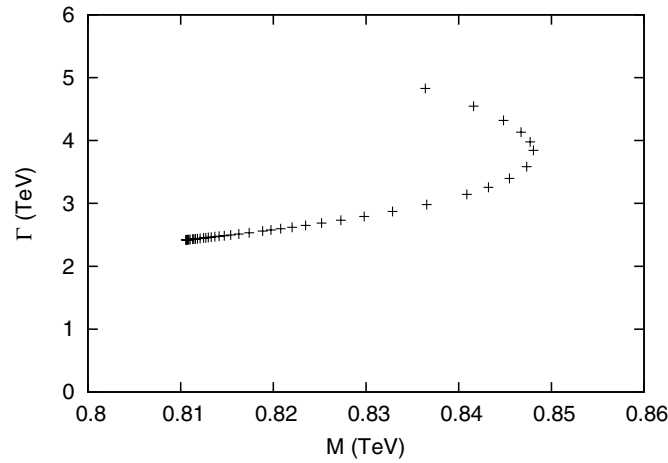


Figure 9. Motion of the pole position $s_0 = (M^2, -M\Gamma)$ of $|t_\omega|$ from equation (45) in the complex s plane for $f \in (250 \text{ GeV}, 6 \text{ TeV})$. For large f , the mass of the very broad ‘resonance’ stabilizes at about 810 GeV, within reach of the LHC, but the width remains huge and the net effect is probably just an enhanced $W_L W_L$ amplitude in the s -wave.

spite of the different mathematical expressions and derivation. Both approximations capture essentially the same physics of the s -channel cut. Moreover, in figure 12, we show the analytical prolongation of the large- N amplitude to the second Riemann sheet where again we can see the above mentioned pole.

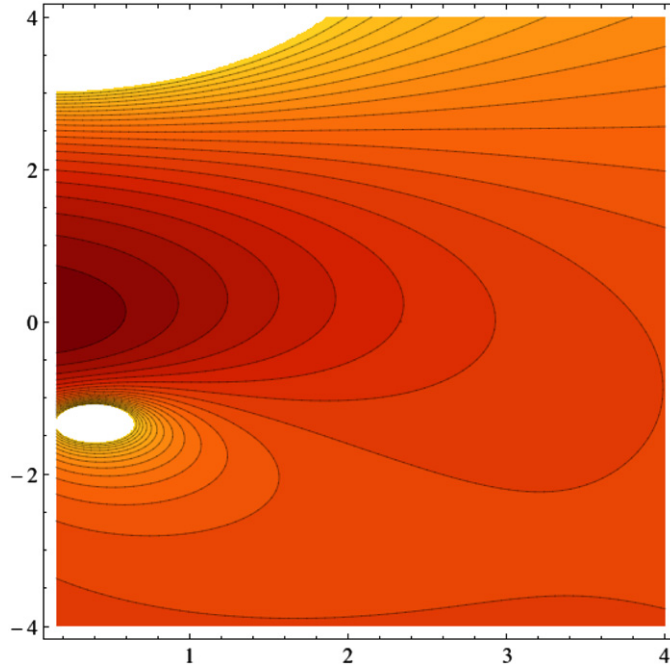


Figure 10. Modulus of the unitarized t_ω in a contour plot in the second Riemann sheet of complex- s . Plotted values range from 0 to 2 (never exceeding 1 for physical s). Note the characteristic pole below the real axis (white circle). Here, $f = 260$ GeV is very close to v , so the strong interaction comes entirely from the coupled channels ($\beta \neq \alpha^2$).

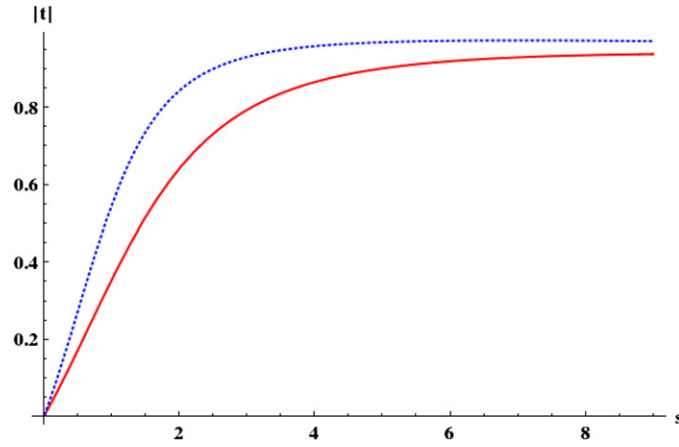


Figure 11. We compare the large- N approximation (top, dashed line) with the K-matrix approximation (bottom, solid line), showing how the moduli of the amplitudes obtained are rather similar. In both cases, only the elastic $\omega\omega \rightarrow \omega\omega$ was included, setting $\beta = 1$ and $f = 0.8$ TeV.

Numerical details cannot be expected to be extremely precise, but neither does the actual experimental situation require it; for exploratory purposes, it is very satisfactory that both approximations yield quite similar results in a strong-interaction scenario where perturbation theory is not applicable.

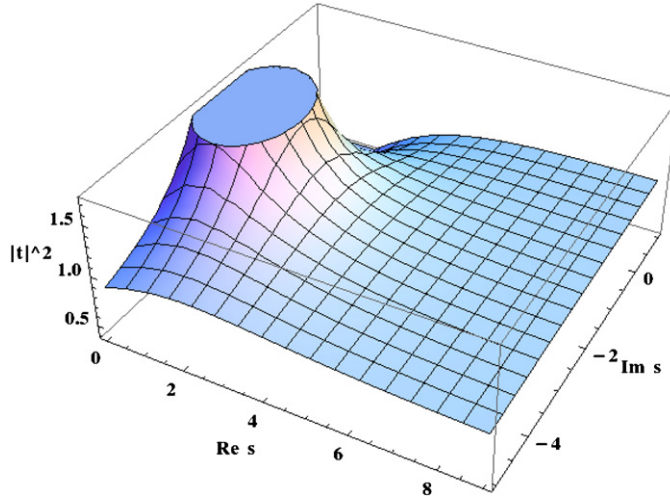


Figure 12. Square modulus of the large- N scattering amplitude t_ω in the second Riemann sheet of complex- s . Note the resonant pole below the real axis. The result is quite analogous to that of figure 7 from the unitarized K matrix amplitude.

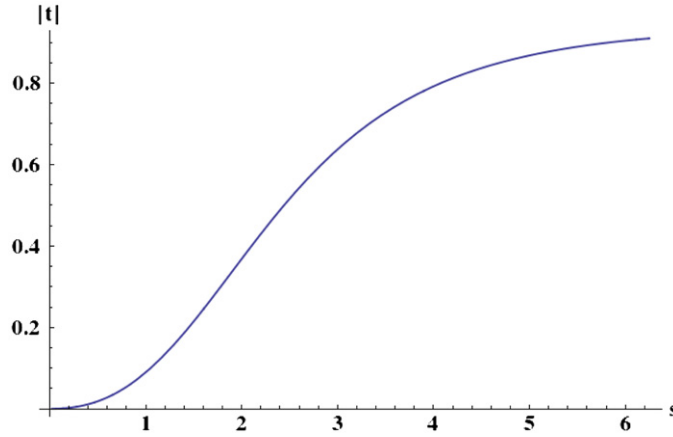


Figure 13. Modulus of \tilde{t}_ω in the N/D method employing the analytical result of subsection 4.3. In this case, we employ $f = 1$ TeV, $\beta = 1$ and we have set the IR cutoff to $m = 150$ GeV.

5.3. Numerical treatment of the N/D method

In figure 13, we show the modulus of the N/D unitarized \tilde{t}_ω in the one-channel case, put together from the explicit analytical solution of subsection 4.3. The strength of the $\omega\omega$ scattering is apparent. The result is very similar to that found, for example, in figure 11, and again it is reassuring that the various sensible unitarization methods yield compatible results. It is also a nice check to look at the imaginary part of the full N/D amplitude in figure 14, showing its characteristic discontinuity at the cut in the first Riemann sheet of the complex s plane.

In figure 15, we show the modulus of the $\omega\omega$ amplitude as function of s for three values of f (in units of v) to show the dependence of the results with this unknown constant. The interactions become indeed strong although unitarity is not quite saturated (with our

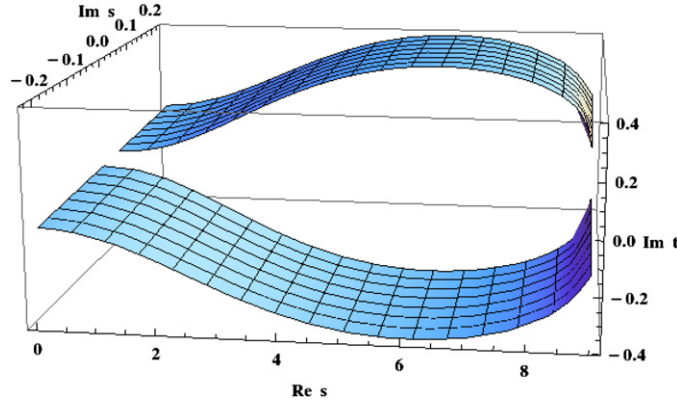


Figure 14. Imaginary part of the elastic amplitude \tilde{t}_ω in the N/D method employing the analytical result of subsection 4.3. Again, $f = 1$ TeV, $\beta = 1$ and $m = 150$ GeV. This view shows the cut on the real s -axis.

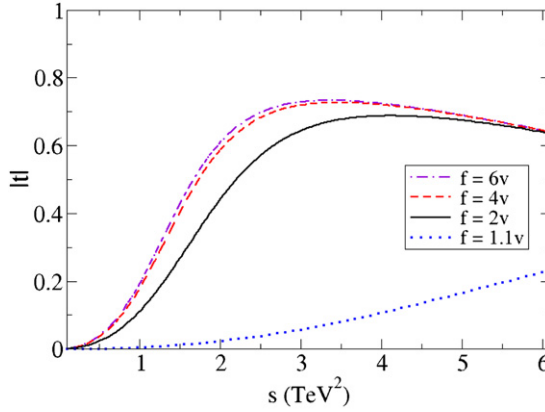


Figure 15. Dependence of t_{00} in the N/D method on the f parameter (scaled by $v = 246$ GeV). We have computed N and D numerically starting $\text{Im}(N)$ from equation (62) in perturbation theory.

normalization this would correspond to $|t| = 1$). Whether or not this happens is model-dependent.

It can be seen that, as $f \rightarrow v$, the amplitude is weaker and any structure recedes to higher energy. In the opposite limit, $f \gg v$, the maximum of the amplitude does not descend below the 1–2 TeV region. The result is in complete analogy to the behavior of the pole in the complex plane analyzed in figure 9.

5.4. The IAM method

Obviously the numerical results coming from the IAM depend on the particular nature of the underlying dynamics through the values of the renormalized EWCHL parameters $a_4(\mu)$ and $a_5(\mu)$ entering in $A(\mu)$. In particular, the IAM unitarized partial wave can be written as:

$$\tilde{t}^\omega = \frac{ks}{1 + \frac{ks}{\pi} \left[\log \frac{-s}{\mu^2} - \frac{\pi}{k^2} \left(A(\mu) + D \log \frac{s}{\mu^2} \right) \right]} \quad (65)$$

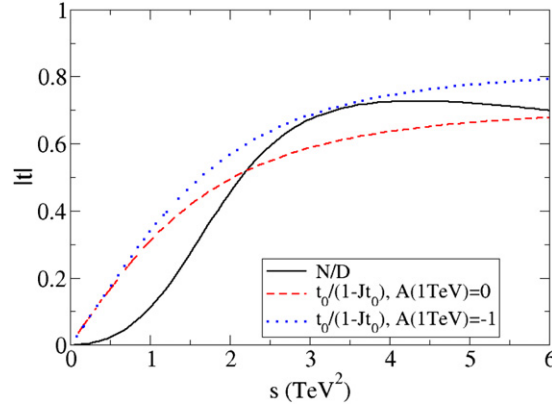


Figure 16. Comparison between the N/D method and a parameterization with a pole as in equation (67) that captures much of the same physics.

as it is very easy to check provided

$$k = \frac{1 - \xi \alpha^2}{16\pi v^2} = \frac{f^2 - \alpha^2 v^2}{16\pi v^2 f^2} \quad (66)$$

or, in other words $t_0^\omega = ks$. We can relate the IAM to the K-matrix single-channel amplitude based on t_0^ω , that was:

$$\tilde{t}^\omega = \frac{ks}{1 + \frac{ks}{\pi} \left(\log \frac{s}{\mu^2} + \log \frac{\mu^2}{\Lambda^2} \right)}, \quad (67)$$

where we have introduced the arbitrary scale μ . This result is obviously simpler than equation (65) and in particular it does not show any LC. However, it could be formally considered a particular case of the IAM result with $D = 0$ and:

$$A(\mu) = \frac{k^2}{\pi} \log \frac{\Lambda^2}{\mu^2}. \quad (68)$$

Therefore, the IAM method improves the simple K-matrix by including the LC and also a contribution to $A(\mu)$ which depends on the dynamics underlying the EWSB. Thus, the possible pole appearing in the second Riemann sheet by using the K-matrix will be modified correspondingly.

In order to roughly understand the behavior of this pole, we can set its position as $s_0 = M^2 - iM\Gamma$ and by choosing $\mu = M$, we get:

$$M^2 = \frac{k}{A(M)} = \frac{16\pi^2 v^2 f^2}{(f^2 - v^2) \log \frac{\Lambda^2}{M^2}}. \quad (69)$$

Thus, with the IAM, we capture the features seen in the plot of the N/D amplitude. As $f \rightarrow v$, its denominator vanishes and the pole position moves to $s = \infty$. But for large f , the pole position becomes saturated and constant, somewhat above 800 GeV, not accessing arbitrarily low energies, and thus avoiding nominal LHC exclusion bounds (though, for such a broad structure, a peak in the spectrum is not really expected). In the opposite limit, $f \rightarrow v$, the pole position moves to large energy and essentially decouples from the low-energy spectrum. The interactions remain weak much longer. A comparison between this toy parameterization and the N/D calculation can be seen in figure 16 for two values of A (a negative quantity).

6. Discussion and summary

In this article, we take as phenomenological input the experimental situation after the first LHC run, namely, the existence of a Higgs-like light scalar resonance (around 125 GeV) and the absence of any other states until about 600 GeV. Therefore, the only light states associated with the electroweak symmetry breaking sector of the Standard Model are the would-be Goldstone bosons responsible for the electroweak boson masses, and this new light scalar resonance.

Extending the philosophy of the electroweak chiral Lagrangians, we have considered the most general low-energy effective Lagrangian with the appropriate symmetries including this new scalar. From this Lagrangian, we have extracted the scattering amplitudes of those scalar bosons, that employing the equivalence theorem for energies $E \gg M_W \sim M_Z$ can be related with the electroweak longitudinal gauge boson scattering.

Excepting the minimal Standard Model case, these amplitudes grow linearly with s (at relatively low energies $E \ll 4\pi v$) and later violate unitarity badly. In consequence, we are forced to introduce some unitarization method. Since there is some controversy about which method is more appropriate (if any), we have explored several well known possibilities, including the K-matrix approach, large- N approximation, N/D and the IAM. Qualitatively, all these methods lead to similar results: a strongly interacting s -wave of $W_L W_L$ scattering, and a pole of the amplitude in the second Riemann sheet.

In the particular case of the Standard Model, there is no term linear in s and the model is weakly interacting, renormalizable and unitary by itself to very good accuracy at the perturbative level because of the lightness of the Higgs mass.

However, it is very important to stress that in general the $W_L W_L$ interactions become strong for most parameter space. In particular, we have found:

- For $\alpha^2 \neq \beta$ and $f > v$, we have strong $W_L W_L$ interactions, and strong coupling with the $\varphi\varphi$ channel.
- For $\alpha^2 = \beta$, $f > v$ strong elastic interactions are expected for $W_L W_L$, and a second, broad scalar analogous to the σ in nuclear physics possibly appears. We identify a pole at 800 GeV or above in the second Riemann sheet very clearly, the question is whether it corresponds to a physical particle since it is so broad⁴.
- Even if $f \simeq v$, with small λ_i , but we allow $\beta > \alpha^2$, one can have strong dynamics resonating between the $W_L W_L$ and $\varphi\varphi$ channels, likewise possibly generating a new scalar pole of the scattering amplitude in the sub-TeV region.
- Finally, as an exception, for $\beta = \alpha^2 = 1$, $f = v$ we recover the MSM with a light Higgs which is weakly interacting.

Since the perturbative interactions grow with s , we have employed several unitarization templates based on the perturbative amplitudes. Unitarization models introduce a systematic error by concentrating on the RC of the amplitudes and only approximating the LC. Still, this is controlled by the fact that the amplitude is wanted for positive s , that is, on the upper lip of the RC. Let us then assess what uncertainty we should expect.

The LC is far in the complex plane, and suppressed by the $s' - s$ denominator that appears in the dispersion relation that ultimately underlies all these models (most clearly seen in the N/D method).

⁴ A second scalar particle S beyond the ‘Higgs’ φ induces two additional terms in the renormalizable \mathcal{L} . For a doublet S , the mass Lagrangian $a\varphi^\dagger\varphi + b(S^\dagger\varphi + \varphi^\dagger S) + cS^\dagger S$ can have a negative eigenvalue for small $a \simeq 0$, $E \simeq \frac{1}{2}(b - \sqrt{b^2 + c^2})$, a possible mechanism for the otherwise ad hoc Mexican-hat potential. For a singlet S , $\lambda|\varphi|^2 S^2$ quartic in the fields can also lead to negative mass term for φ , if S acquires a vacuum expectation value (e.g., dilatation symmetry breaking) and $\lambda < 0$, acceptable if the quartic couplings of S and φ themselves are large enough.

Our perturbative treatment of the LC is reliable to a typical $s \propto -(4\pi f)^2$, so the relative error incurred on that LC is not of order 1 before then. We are interested in the unitarized amplitude for $s \propto (4\pi f)^2$ on the physical RC (for smaller s there is no need to unitarize anything, the perturbative counting will do as well). The variation of \tilde{t}^ω on the RC has as typical scale f . We expect that the integral over the RC will be dominated by an interval of width f around the given s where the amplitude is wanted. Thus, we expect the unitarization methods to have a typical relative error $f/(2 \times 4\pi f) \sim 1/(8\pi)$, or at the 5–10% level. In order to assess this systematic error, we have employed different unitarization methods and found qualitatively similar results.

We have insisted that the pole we find in the second Riemann sheet of the WBGB scattering amplitude can only with difficulty be interpreted as a physical state. This is because the structure is very broad and its main role is to make interactions strong. Other authors have reported new possible scalar states, for example in lattice calculations [41] involving Higgs–Higgs dynamics.

Finally, it remains to address a philosophical question. If one takes as ultimate guiding principle the renormalizability of the theory, one finds the MSM, with a very specific choice of parameters ($f = v$, $\alpha = \beta = 1$) and higher energy scattering of longitudinal vector bosons will be weak. Instead, if one adopts the effective theory way of thinking, where all possible low-energy couplings are allowed in the Lagrangian and need to be measured, then one finds that most likely scattering will be strong.

Ultimately, the observation by Wilson that only relevant operators remain in the low-energy theory after integrating out high-momentum shells, implies that whoever adopts the first, *renormalizable* point of view, is already committing to any new physics being at a very high scale.

Instead, he who adopts the second possibility, for example that dilatation invariance is broken by f at a higher energy scale than electroweak invariance is broken by v , is implicitly assuming that some new physics (that we find to be strong interactions and possibly a second scalar resonance) is not too far in energy.

There is no current empirical information allowing us to choose one or another alternative, so at the present time, it is largely a matter of personal taste. We look forward to further LHC data guiding theory.

Acknowledgments

FJLE thanks the hospitality of the NEXT institute and the high energy group at the University of Southampton, ADG thanks the CERN-TH, and both the hospitality of the ECT* at Trento during the final stages of this work. This work was supported by Spanish grant FPA2011-27853-C02-01 and by the grant BES-2012-056054 that supports RDL.

Appendix. Dispersive integrals

In order to compute the dispersive integrals necessary for the algebraic treatment of the N/D method in subsection 4.3, we consider the more general IR and UV regularized integrals:

$$I = \int_{m^2}^{\Lambda^2} \frac{ds' f(s')}{s' - s - i\epsilon}, \quad (\text{A.1})$$

where $s, s' \in (m^2, \Lambda^2)$ and $f(s')$ is analytic around this interval. By using the well known distribution identity:

$$\frac{1}{s' - s - i\epsilon} = PV \frac{1}{s' - s} + i\pi \delta(s' - s) \quad (\text{A.2})$$

one has

$$I = PV[I] + i\pi f(s) \quad (\text{A.3})$$

where PV stands for Cauchy's principal value part, i.e.

$$\begin{aligned} PV[I] &= \lim_{\epsilon \rightarrow 0} \left(\int_{m^2}^{s-\epsilon} \frac{ds' f(s')}{s' - s} + \int_{s+\epsilon}^{\Lambda} \frac{ds' f(s')}{s' - s} \right) \\ &= g(\Lambda^2, s) - g(m^2, s) - \lim_{\epsilon \rightarrow 0} (g(s + \epsilon, s) - g(s - \epsilon, s)) \end{aligned} \quad (\text{A.4})$$

where $g(s', s)$ is a primitive of $f(s')/(s' - s)$, that is,

$$\frac{\partial g(s', s)}{\partial s'} = \frac{f(s')}{s' - s}. \quad (\text{A.5})$$

Now, since by hypothesis f is analytic in a domain surrounding s , it is possible to expand $f(s')$ around s as:

$$f(s') = f(s) + f'(s)(s' - s) + \frac{1}{2}f''(s)(s' - s)^2 + \dots \quad (\text{A.6})$$

yielding the Laurent series

$$\frac{f(s')}{s' - s} = \frac{f(s)}{s' - s} + f'(s) + \frac{1}{2}f''(s)(s' - s) + \dots \quad (\text{A.7})$$

and then we can choose $g(s', s)$ as:

$$g(s', s) = f(s) \log(s' - s) + f'(s)(s' - s) + \frac{1}{4}f''(s)(s' - s)^2 + \dots \quad (\text{A.8})$$

Therefore:

$$\begin{aligned} PV[I] &= g(\Lambda^2, s) - g(m^2, s) - \lim_{\epsilon \rightarrow 0} \left[f(s) \log \frac{\epsilon}{-\epsilon} + f'(s)2\epsilon + O(\epsilon^3) \right] \\ &= g(\Lambda^2, s) - g(m^2, s) - i\pi f(s) \end{aligned} \quad (\text{A.9})$$

and canceling $i\pi f(s)$ upon substitution in equation (A.3) we finally obtain the simple relation

$$I = \int_{m^2}^{\Lambda^2} \frac{ds' f(s')}{s' - s - i\epsilon} = g(\Lambda^2, s) - g(m^2, s) \quad (\text{A.10})$$

for any $g(s', s)$ satisfying equation (A.5). By using this result it is not difficult to compute the integrals needed in subsection 4.3. Some of them involve the dilogarithm function $Li_2(z)$ defined for $|z| < 1$ as

$$Li_2(z) = \sum_{n=1}^{\infty} \frac{z^n}{n^2} \quad (\text{A.11})$$

and extended analytically for other values of z by the integral form of that series

$$Li_2(z) = - \int_0^z dt \frac{\log(1-t)}{t}. \quad (\text{A.12})$$

Note the particular values $Li_2(0) = 0$ and $Li_2(1) = \pi^2/6$. For very large z we also recall the very useful asymptotic behavior

$$Li_2(z) \simeq \frac{\pi^2}{6} - \frac{1}{2} \log^2(-z). \quad (\text{A.13})$$

A key property of the family of I integrals in equation (A.10) is that all of them can be analytically extended to the whole complex plane. In particular, $Li_2(z)$ is analytic except for a cut on the positive real axis starting from $z = 1$, so that $\text{Im } Li_2(|z| + i\epsilon) = \pi \log |z| \theta(|z| - 1)$. Thus, equation (A.10) allows the explicit computation of the N/D amplitude presented in subsection 4.3 since the tree-level amplitudes are simple enough that the g -primitives can be found by inspection or with a simple symbolic manipulation program.

References

- [1] Chatrchyan S *et al* (CMS Collaboration) 2012 *Phys. Lett. B* **716** 30
- [2] Aad G *et al* (ATLAS Collaboration) 2012 *Phys. Lett. B* **716** 1
- [3] Aad G *et al* (ATLAS Collaboration) 2012 *Report No. ATLAS-CONF-2012-168*
Chatrchyan S *et al* (CMS Collaboration) 2012 *Report No. CMS-HIG-12-015*
- [4] Aad G *et al* (ATLAS Collaboration) 2013 *Phys. Lett. B* **726** 88 (arXiv:1307.1427 [hep-ex])
- [5] (CMS Collaboration) 2012 *Collaboration report CMS-PAS-HIG-12-045*
- [6] Chatrchyan S *et al* (CMS Collaboration) 2012 *Phys. Lett. B* **710** 26
Aad G *et al* (ATLAS Collaboration) 2012 *Phys. Lett. B* **716** 1
Einsweiler K (ATLAS Collaboration) 2012 *Eur. Phys. J. HCP Symp.(Kyoto)*; (to be published)
Paus C (CMS Collaboration) 2012 *Eur. Phys. J. HCP Symp. (Kyoto)*; (to be published)
- [7] Appelquist T and Bernard C 1980 *Phys. Rev. D* **22** 200
Longhitano A 1980 *Phys. Rev. D* **22** 1166
Longhitano A 1981 *Nucl. Phys. B* **188** 118
Dobado A, Espriu D and Herrero M J 1991 *Phys. Lett. B* **255** 405
Holdom B and Terning J 1990 *Phys. Lett. B* **247** 88
Dobado A, Espriu D and Herrero M J 1991 *Phys. Lett. B* **255** 405
Golden M and Randall L 1991 *Nucl. Phys. B* **361** 3
- [8] Weinberg S 1979 *Physica A* **96** 327
Gasser J and Leutwyler H 1984 *Ann. Phys.* **158** 142
Gasser J and Leutwyler H 1985 *Nucl. Phys. B* **250** 465–517
- [9] Cornwall J M, Levin D N and Tiktopoulos G 1974 *Phys. Rev. D* **10** 1145
Vayonakis C E 1976 *Lett. Nuovo Cimento* **17** 383
Lee B W, Quigg C and Thacker H 1977 *Phys. Rev. D* **16** 1519
Chanowitz M S and Gaillard M K 1985 *Nucl. Phys.* **261** 379
Dobado A and Peláez J R 1994 *Nucl. Phys. B* **425** 110
Dobado A and Peláez J R 1994 *Phys. Lett. B* **329** 469
Dobado A and Peláez J R 1994 *Phys. Lett. B* **335** 554 (addendum)
- [10] Belyaev A 2013 private communication
- [11] Contino R, Grojean C, Moretti M, Piccinini F and Rattazzi R 2010 *J. High Energy Phys. JHEP05(2010)089* (arXiv:1002.1011 [hep-ph])
Contino R 2010 arXiv:1005.4269 [hep-ph]
Grober R and Muhlleitner M 2011 *J. High Energy Phys. JHEP06(2011)020* (arXiv:1012.1562 [hep-ph])
Alonso R *et al* 2013 *Phys. Lett. B* **722** 330 (arXiv:1212.3305 [hep-ph])
- [12] Kaplan D B and Georgi H 1984 *Phys. Lett. B* **136** 183
Dimopoulos S and Preskill J 1982 *Nucl. Phys. B* **199** 206
Banks T 1984 *Nucl. Phys. B* **243** 125
Kaplan D B, Georgi H and Dimopoulos S 1984 *Phys. Lett. B* **136** 187
Georgi H, Kaplan D B and Galison P 1984 *Phys. Lett. B* **143** 152
Georgi H and Kaplan D B 1984 *Phys. Lett. B* **145** 216
Dugan M J, Georgi H and Kaplan D B 1985 *Nucl. Phys. B* **254** 299
Giudice G F, Grojean C, Pomarol A and Rattazzi R 2007 *J. High Energy Phys. JHEP06(2007)045* (arXiv:hep-ph/0703164)
- [13] Pich A, Rosell I and Sanz-Cillero J J 2013 arXiv:1307.1958 [hep-ph]
- [14] Halyo E 1993 *Mod. Phys. Lett. A* **8** 275
Goldberger W D, Grinstein B and Skiba W 2008 *Phys. Rev. Lett.* **100** 111802 (arXiv:0708.1463 [hep-ph])
- [15] Truong T N 1988 *Phys. Rev. Lett.* **61** 2526
Dobado A, Herrero M J and Truong T N 1990 *Phys. Lett. B* **235** 134
- [16] Dobado A and Peláez J R 1993 *Phys. Rev. D* **47** 4883 (arXiv:hep-ph/9301276)
Dobado A and Peláez J R 1994 *Nucl. Phys. B* **425** 110
Dobado A and Peláez J R 1995 *Nucl. Phys. B* **434** 475 (arXiv:hep-ph/9401202) (erratum)
- [17] Oller J A and Oset E 2000 *Nucl. Phys. A* **663** 629 (arXiv:hep-ph/9908495)
- [18] Azatov A, Contino R and Galloway J 2012 *J. High Energy Phys. JHEP04(2012)127*
Azatov A, Contino R and Galloway J 2013 *J. High Energy Phys. JHEP04(2013)140* (arXiv:1202.3415 [hep-ph]) (erratum)
- [19] Belanger G *et al* 2013 arXiv:1306.2941 [hep-ph]

- Corbett T *et al* 2012 *Phys. Rev. D* **86** 075013 (arXiv:1207.1344 [hep-ph])
 Corbett T *et al* 2013 arXiv:1306.0006 [hep-ph]
 Ellis J and You T 2013 arXiv:1303.3879 [hep-ph]
 Giardino P P *et al* 2013 arXiv:1303.3570 [hep-ph]
 Falkowski A, Riva F and Urbano A 2013 (arXiv:1303.1812 [hep-ph])
- [20] Glashow S L 1961 *Nucl. Phys.* **22** 579
 Weinberg S 1967 *Phys. Rev. Lett.* **19** 1264
 Salam A ed N Svartholm 1968 *Proc. 8th Nobel Symp.* (Stockholm: Almqvist) p 367
- [21] Agashe K, Contino R and Pomarol A 2005 *Nucl. Phys. B* **719** 165 (arXiv:hep-ph/0412089)
 Contino R, Da Rold L and Pomarol A 2007 *Phys. Rev. D* **75** 055014 (arXiv:hep-ph/0612048)
- [22] Chanowitz M S, Golden M and Georgi H 1987 *Phys. Rev. D* **36** 1490
- [23] Dobado A and Herrero M J 1989 *Phys. Lett. B* **228** 495
 Dobado A and Herrero M J 1989 *Phys. Lett. B* **233** 505
 Donoghue J and Ramirez C 1990 *Phys. Lett. B* **234** 361
- [24] Delgado R L, Dobado A and Llanes-Estrada F J arXiv:1311.5993 [hep-ph]
- [25] Espriu D, Mescia F and Yenchon B 2013 arXiv:1307.2400 [hep-ph]
- [26] Gupta S N 1981 *Quantum Electrodynamics* (New York, NY: Gordon and Breach) pp 191–198
- [27] Aydemir U, Anber M M and Donoghue J F 2012 *Phys. Rev. D* **86** 014025 (arXiv:hep-ph/1203.5153)
- [28] Oller J A and Oset E 1999 *Phys. Rev. D* **60** 074023 (arXiv:hep-ph/9809337)
- [29] Coleman S, Jackiw R and Politzer H D 1974 *Phys. Rev. D* **10** 2491
 Coleman S 1985 *Aspects of Symmetry* (Cambridge: Cambridge University Press)
 Casalbuoni R, Dominici D and Gatto R 1984 *Phys. Lett. B* **147** 419
 Einhorn M B 1984 *Nucl. Phys. B* **246** 75
 Dobado A, Morales J, Pelaez J R and Urdiales M T 1996 *Phys. Lett. B* **387** 563 [hep-ph/9607369]
 Morales J, Hurtado R, Martinez R and Diaz R A 2005 *Braz. J. Phys.* **35** 597
- [30] Dobado A and Pelaez J R 1992 *Phys. Lett. B* **286** 136
- [31] Chew G F and Mandelstam S 1960 *Phys. Rev.* **119** 467
- [32] Hikasa K and Igi K 1993 *Phys. Rev. D* **48** 3055
- [33] Dobado A, Herrero M J and Truong T N 1990 *Phys. Lett. B* **235** 134
 Dobado A and Pelaez J R 1993 *Phys. Rev. D* **47** 4883
 Oller J A, Oset E and Pelaez J R 1998 *Phys. Rev. Lett.* **80** 3452
 Oller J A, Oset E and Pelaez J R 1999 *Phys. Rev. D* **59** 074001
 Oller J A, Oset E and Pelaez J R 1999 *Phys. Rev. D* **60** 099906
 Oller J A, Oset E and Pelaez J R 2007 *Phys. Rev. D* **75** 099903
 Guerrero F and Oller J A 1999 *Nucl. Phys. B* **537** 459
 Oller J A, Oset E and Pelaez J R 2001 *Phys. Rev. D* **60** 641
 Dobado A and Pelaez J R 2002 *Phys. Rev. D* **65** 077502
- [34] Dobado A, Herrero M J and Truong T N 1990 *Phys. Lett. B* **235** 129
 Dobado A, Herrero M J and Truong T N 1990 *Phys. Lett. B* **235** 129
 Dicus D A and Repko W W 1990 *Phys. Rev. D* **42** 3660
 Dicus D A and Repko W W 1991 *Phys. Rev. D* **44** 3473
 Dicus D A and Repko W W 1993 *Phys. Rev. D* **47** 4154
 Pelaez J R 1997 *Phys. Rev. D* **55** 4193
- [35] Dobado A *et al* 1997 *Effective Lagrangians for the Standard Model* (Heidelberg: Springer)
- [36] Nicola A Gomez, Pelaez J R and Rios G 2008 *Phys. Rev. D* **77** 056006 (arXiv:0712.2763 [hep-ph])
- [37] Espriu D and Yenchon B 2012 arXiv:1212.4158v2 [hep-ph]
- [38] Grinstein B and Trott M 2007 *Phys. Rev. D* **76** 073002 (arXiv:0704.1505 [hep-ph])
- [39] Alboteanu A, Kilian W and Reuter J 2008 *J. High Energy Phys.* **JHEP11(2008)010** (arXiv:0806.4145 [hep-ph])
- [40] Reuter J, Kilian W and Sekulla M 2013 arXiv:1307.8170 [hep-ph]
- [41] Maas A 2012 arXiv:1205.6625 [hep-lat]
 Maas A and Mufti T 2012 arXiv:1211.5301 [hep-lat]
- [42] Turton D 2013 *Springer Proc. Phys.* **144** 255–6
- [43] Buchalla G, Cata O and Krause C 2013 arXiv:1307.5017 [hep-ph]